PROCEEDINGS OF SCIENCE

HERA Collider Results

A M Cooper-Sarkar*
Oxford University
E-mail: amanda.cooper-sarkar@physics.ox.ac.uk

The final results on the combination of all inclusive deep-inelastic scattering cross section data from the H1 and ZEUS experiments at HERA are reviewed. The parton distribution functions (PDFs) extracted from these data (HERAPDF2.0) and from HERA data on heavy flavour production and jet production are also presented (HERAPDF2.0Jets). The use of various heavy flavour schemes is compared and the sensitivity of the data to cuts on Q^2 is explored. When jet data are included in the fits, a competitive value $\alpha_s(M_Z^2) = 0.1184 \pm 0.0016$ is extracted at NLO, excluding scale uncertainties

XXIII International Workshop on Deep-Inelastic Scattering,
27 April - May 1 2015
Dallas, Texas

*Speaker.

PoS(DIS2015)005

1. Introduction

Deep inelastic scattering (DIS) of electrons and positrons on protons at HERA has been central to the exploration of proton structure and quark-gluon interaction dynamics as described by perturbative Quantum Chromo Dynamics (pQCD). HERA was operated at a centre-of-mass energy of up to $\sqrt{s} \simeq 320\,\text{GeV}$. This enabled the two collaborations, H1 and ZEUS, to explore a large phase space in Bjorken x, x_{Bj}, and negative four-momentum-transfer squared, Q^2. Cross sections for neutral current (NC) interactions were published for $0.045 \leq Q^2 \leq 50000\,\text{GeV}^2$ and $6 \cdot 10^{-7} \leq x_{Bj} \leq 0.65$.

HERA was operated in two phases: HERA I, from 1992 to 2000, and HERA II, from 2002 to 2007. It was operated with an electron beam energy of $E_e \simeq 27.5\,\text{GeV}$. For most of HERA I and II, the proton beam energy was $E_p = 920\,\text{GeV}$, resulting in the highest centre-of-mass energy of $\sqrt{s} \simeq 320\,\text{GeV}$. During all of HERA running, the H1 and ZEUS collaborations collected total integrated luminosities of approximately $500\,\text{pb}^{-1}$ each, divided about equally between e^+p and ep scattering. The data presented here is the final combination of HERA inclusive data based on all published H1 and ZEUS measurements corrected to zero beam polarisation. This includes data taken with proton beam energies of $E_p = 920$, 820, 575 and 460 GeV corresponding to at $\sqrt{s} \simeq 320$, 300, 251 and 225 GeV.

The combination was performed using the package HERAverager [1] and the pQCD analysis using HERAFitter [2]. The correlated systematic uncertainties and global normalisations were treated such that one coherent data set was obtained. The combination leads to a significantly reduced uncertainty compared to the orginal inputs and compared to the previous combination of HERA-I data, particularly in the electron sector, see Fig. 1. The combined data demonstrate electroweak unification beautifully and allow an extraction of $xF_3^{\gamma Z}$, see Fig. 2

Within the framework of pQCD, the proton is described by parton distribution functions (PDFs) which provide probabilities for a particle to scatter off partons, gluons or quarks, carrying the fraction x of the proton momentum. Perturbative QCD determines the evolution of the PDFs to any scale once they are provided at a starting scale. The name HERAPDF stands for a pQCD analysis, within the DGLAP formalism, to determine the PDFs at the starting scale by fitting the x_{Bj} and Q^2 dependences of the combined HERA NC and CC DIS cross sections. The name HERAPDF2.0 refers to this analysis based on the newly combined inclusive DIS cross sections from all of HERA I and HERA II. The strength of the HERAPDF approach is that one coherent high-precision data set containing NC and CC cross sections is used as input. The newly combined data entering the HERAPDF2.0 analysis span four orders of magnitude in Q^2 and x_{Bj}. The availability of precision NC and CC cross sections over such a large large phase space allows HERAPDF to be based on ep scattering data only and makes HERAPDF independent of any nuclear corrections. The difference between the NC e^+p and e^-p cross sections at high Q^2, together with the high-Q^2 CC data, constrain the valence quark distributions. The CC data also constrain the down sea-quark distribution in the proton without assuming isospin symmetry. The lower-Q^2 NC data constrain the low-x sea-quark distributions. The precisely measured Q^2 variations of the DIS cross sections in different bins of x_{Bj} constrain the gluon distribution. Measurement of cross sections at different beam energies constrains the longitudinal structure function, F_L, and thus provides independent information on the gluon distribution.

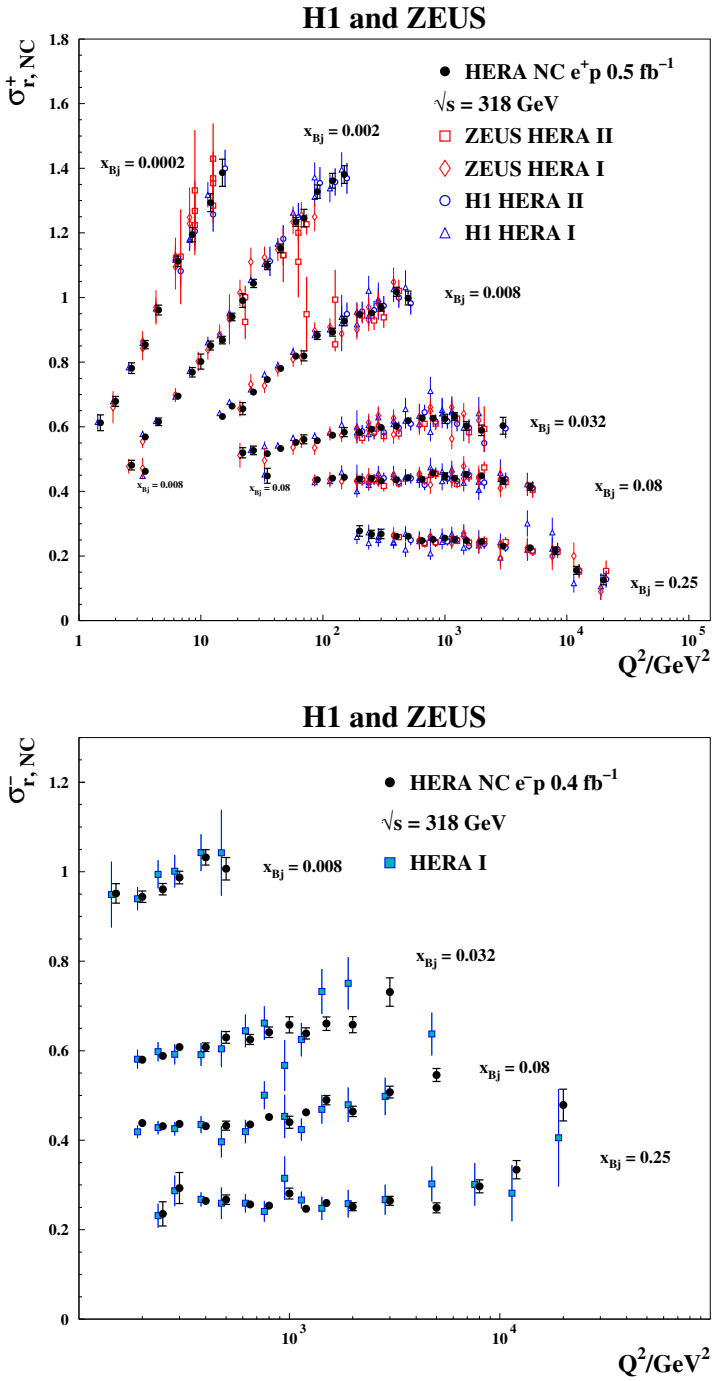

Figure 1: HERA combined NC e^+p reduced cross sections as a function of Q^2 for selected x_{Bj}-bins compared to the individual H1 and ZEUS data(top); and HERA combined NC e^-p reduced cross sections compared to the to the HERA-I combination (bottom).

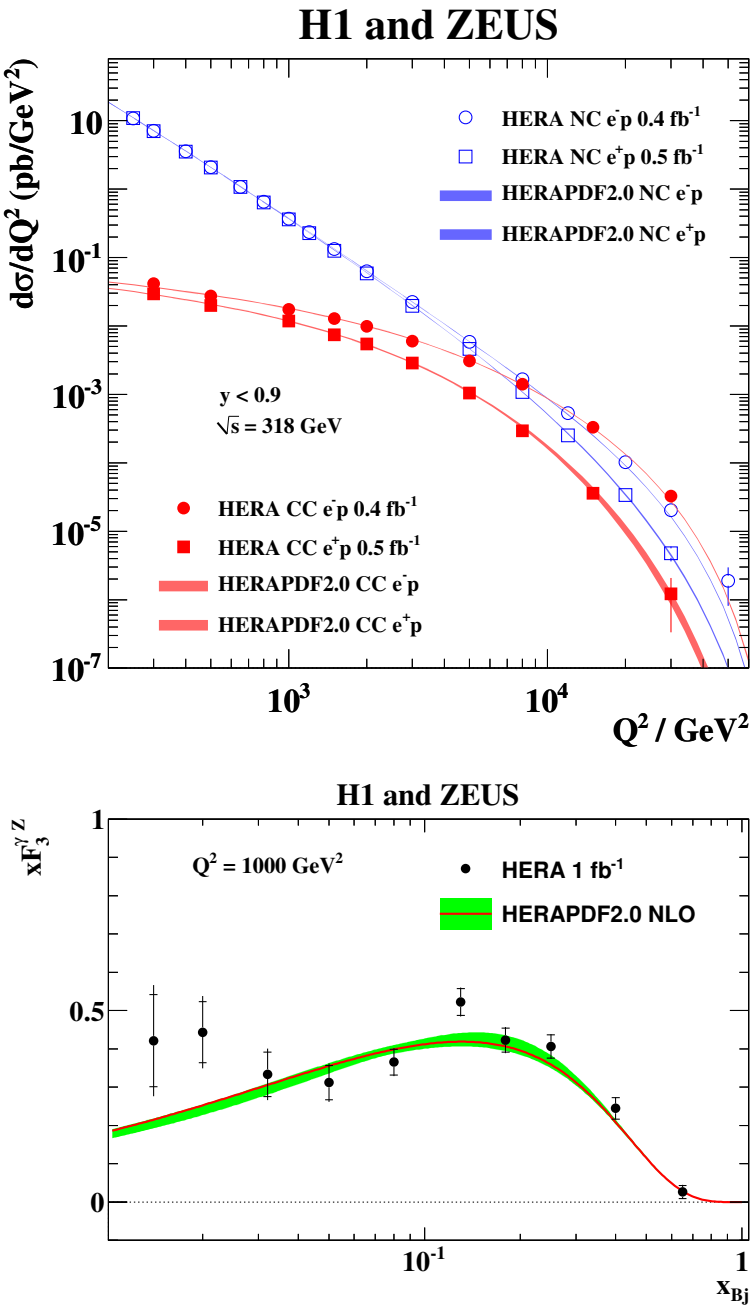

Figure 2: NC and CC e^-p and e^+p cross sections (top) The structure function $xF_3^{\gamma Z}$ at $Q^2 = 1000\,\mathrm{GeV}^2$ (bottom). The data are compared with the prediction from HERAPDF2.0 NLO.

The consistency of the input data allowed the determination of the experimental uncertainties on the HERAPDF2.0 parton distributions using rigorous statistical methods. Uncertainties resulting from model assumptions and from the choice of the parameterisation of the PDFs are considered separately.

Both H1 and ZEUS also published charm-production cross sections, which were combined and analysed previously, as well as jet-production cross sections. These data were included to obtain a variant HERAPDF2.0Jets. The inclusion of jet cross-sections made it possible to simultaneously determine the PDFs and the strong coupling constant $\alpha_s(M_Z^2)$. Full details of the analysis are given in ref. [3].

2. HERAPDF2.0 and its variations

Fig. 3 shows summary plots at $\mu_f = 10\text{GeV}^2$ of the valence, total Sea and gluon PDFs for HERAPDF2.0 analysed at NLO and at NNLO, for the standard cut $Q^2 > 3.5\text{GeV}^2$. The experimental uncertainties are shown in red. Model uncertainties are shown in yellow. These are due to variation of the central choices for: the Q^2 cut; the values of the pole-masses of the charm and beauty quarks; the fractional contribution and the shape of the strange-PDF. HERA data on charm and beauty production determine the central choices of the heavy quark masses and their model variations. Parametrization uncertainties are shown in green. These are due to: variation of the starting scale; addition of extra parameters. The central choice of parametrization is determined as usual for HERAPDF analyses by saturation of the χ^2, but the addition of extra parameters sometimes results in close-by but distinct minima. Additionally seen on these figures is the result of an alternative gluon parametrisation HERAPDF2.0AG, for which the gluon must be positive definite for all Q^2 above the starting scale. These PDFs are similar in χ^2 to the standard ones at NLO but are disfavoured at NNLO. An LO set is also available using the alternative gluon parametrisation. It is shown compared to the NLO set in Fig. 4. The standard fits use a value of the strong coupling constant, $\alpha_s(M_Z^2) = 0.118$, at NLO and NNLO, and, $\alpha_s(M_Z^2) = 0.130$, at LO, but sets using a range of values from 0.110 to 0.130 are also available.

A more extreme variation of the Q^2 cut, $Q^2 > 10\text{GeV}^2$, has also been considered, resulting in the HERAPDF2.0HiQ2 PDFs, since it was observed that the χ^2 per degree of freedom of the fit decreases steadily until $Q^2 > 10\text{GeV}^2$. This is true for both NLO and NNLO fits and it is true independent of the heavy quark scheme used to analyse the data, see Fig. 5. In fact it depends mostly on the order to which F_L is evaluated. The fits do not favour the evaluation of F_L to $O(\alpha_s^2)$. It is also somewhat counter-intuitive that the χ^2 is not improved when going from NLO to NNLO within the same scheme, the fits do not favour the faster NNLO evolution.

HERA kinematics are such that low Q^2 is also low x. Thus HERAPDF2.0HiQ2 PDFs are used to assess any bias resulting from the inclusion of low-Q^2, low-x data which might require analysis beyond the DGLAP formalism, such as: resummation of $ln(1/x)$ terms, non-linear evolution equations and non-perturbative effects. Figs. 6 show that there is no bias at high scale due to the inclusion of the lower Q^2 data.

Figs 7 compare the HERAPDF2.0NLO fit to the HERAPDF1.0NLO fit. One can see the reduction in the high-x uncertainties and the fact that the high-x Sea is now much less hard. Figs. 8 make the same comparison for the HERAPDF2.0NNLO and the HERAPDF1.5NNLO fit. Again

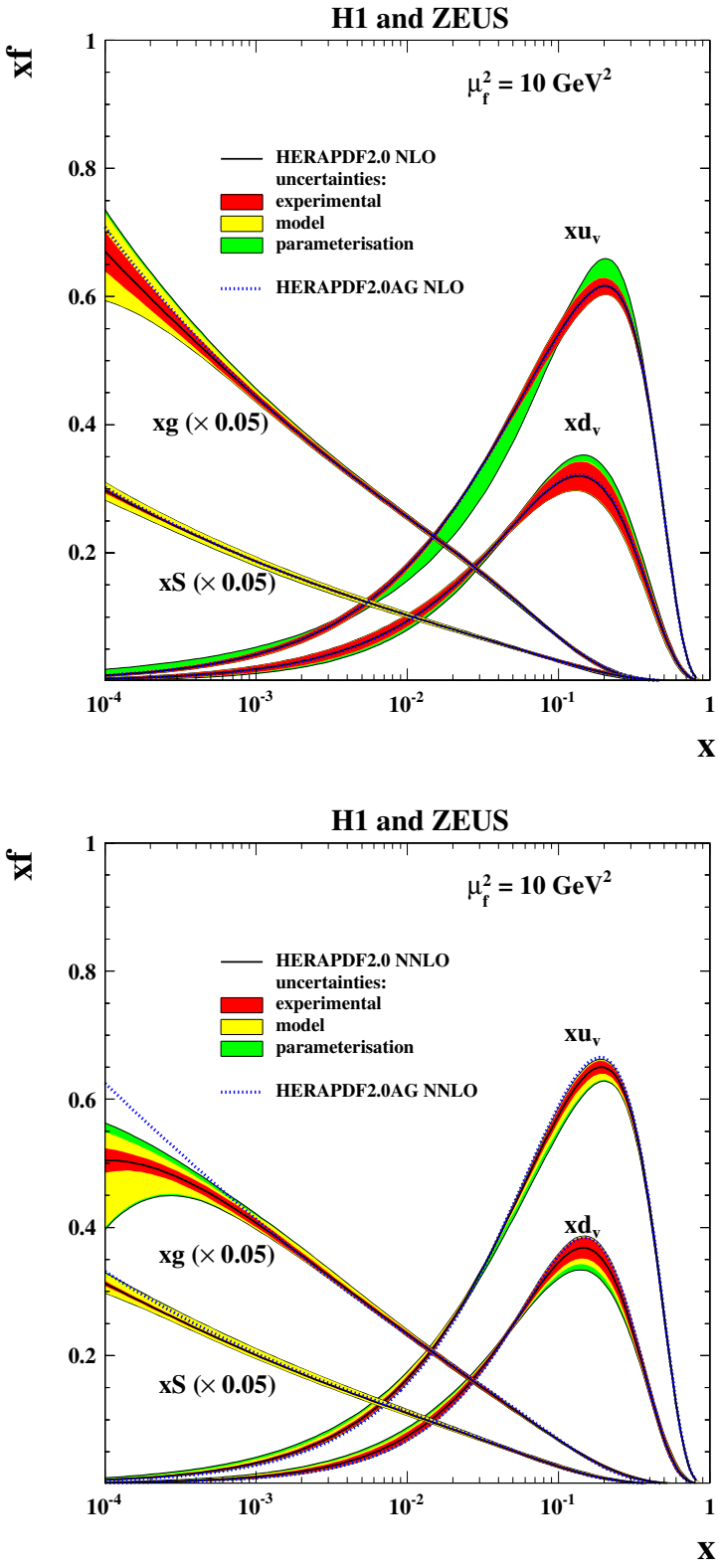

Figure 3: The parton distribution functions of HERAPDF2.0 NLO(top) and NNLO(bottom), xu_v, xd_v, $xS = 2x(\bar{U}+\bar{D})$, xg, at $\mu_f^2 = 10\,\mathrm{GeV}^2$. The gluon and sea distributions are scaled down by a factor of 20. The experimental, model and parameterisation uncertainties are shown separately. The dotted lines represent HERAPDF2.0AG NLO with an alternative gluon parameterisation.

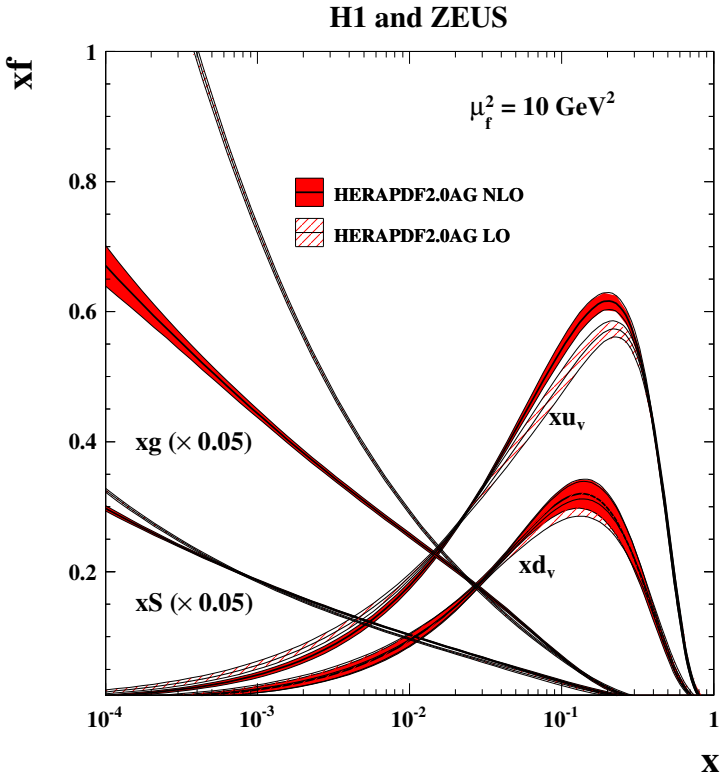

Figure 4: HERAPDF2.0 PDFs at LO and NLO are compared using experimental uncertaities only. The alternative gluon form of the parametrisation is used for both.

the high-x uncertainty is reduced and in particular, the high-x gluon has a much reduced uncertainty band and its central value moves towards the lower end of the HERAPDF1.5 uncertainty band.

Two sets of PDFs using a fixed flavour number scheme have been extracted, as shown in Fig 9. These differ from each other in three respects: the order at which F_L is evaluated $O(\alpha_s^2)$ (FF3A), $O(\alpha_s)$ (FF3B); whether or not α_s runs with 3-flavours (FF3A) or with variable flavour (FF3B); and the use of pole masses (FF3A) or current masses (FF3B).

Heavy flavour data from the charm combination has also been added to the fit, but it does not make much difference once its constraining effect on the charm mass has been taken into account. Adding data on jet productuion also does not make much difference IF the value of $\alpha_s(M_Z^2)$ is kept fixed. However if $\alpha_s(M_Z^2)$ is free then jet data have a dramatic effect in constraining its value, see Fig. 10, where the χ^2 profiles vs $\alpha_s(M_Z^2)$ are shown for the NLO and NNLO fits to inclusive data alone and the same profile is shown for the NLO fit including jets. (Note that we cannot include jets in an NNLO fit since jet production cross sections in DIS have not been calculated to NNLO). A simultaneous fit of the PDFs and the value of $\alpha_s(M_Z^2)$ can be made once the jet data are included resulting in the value, $\alpha_s(M_Z^2) = 0.1183 \pm 0.009(exp) \pm 0.0005(model/param) \pm 0.0012(had)^{+0.0037}_{-0.0030}(scale)$, where 'had' indicates extra uncertainties due to the hadronisation of the jets. The gluon PDF is strongly correlated to the value of $\alpha_s(M_Z^2)$ and thus, in a fit where $\alpha_s(M_Z^2)$ is free, the gluon uncertainty increases. However, provided that jet data are included in the fit this increase is not dramatic, see Figs 11.

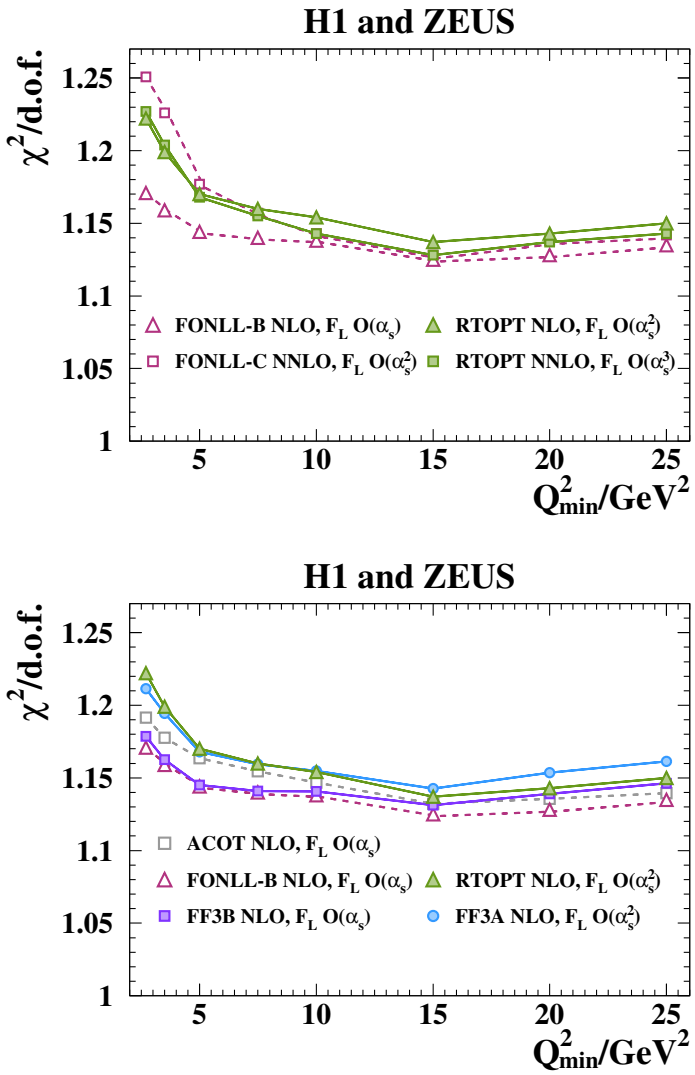

Figure 5: The dependence of $\chi^2/d.o.f$ on Q^2_{min} for HERAPDF2.0 fits: (top) using the RTOPT and FONLL schmes at NLO and NNLO; (bottom) using RTOPT, ACOT and FONLL-B schemes and fixed flavour number schemes at NLO.

3. Conclusions

The H1 and ZEUS data on inclusive $e^{\pm}p$ neutral and charged current cross sections have been combined into a data set with a total integrated luminosity of $\sim 1fb^{-1}$. This data set spans six orders of magnitude in both x and Q^2. The combined cross sections were used as input to a pQCD analysis to extract the parton distribution functions HERAPDF2.0 at LO, NLO and NNLO. The effect of using various different heavy flavour schemes and different Q^2 cuts on the data was investigated. All heavy flavour schemes show some sensitivity to the minimim Q^2 cut, however the choice of this cut does not bias data at high scale significantly. For the standard fits the value of $\alpha_s(M_Z^2)$ is fixed, but a measurement of $\alpha_s(M_Z^2)$ can be made if jet data are included in the fit, resulting in the value $\alpha_s(M_Z^2) = 0.1184 \pm 0.0016$ at NLO, excluding scale uncertainties. The data

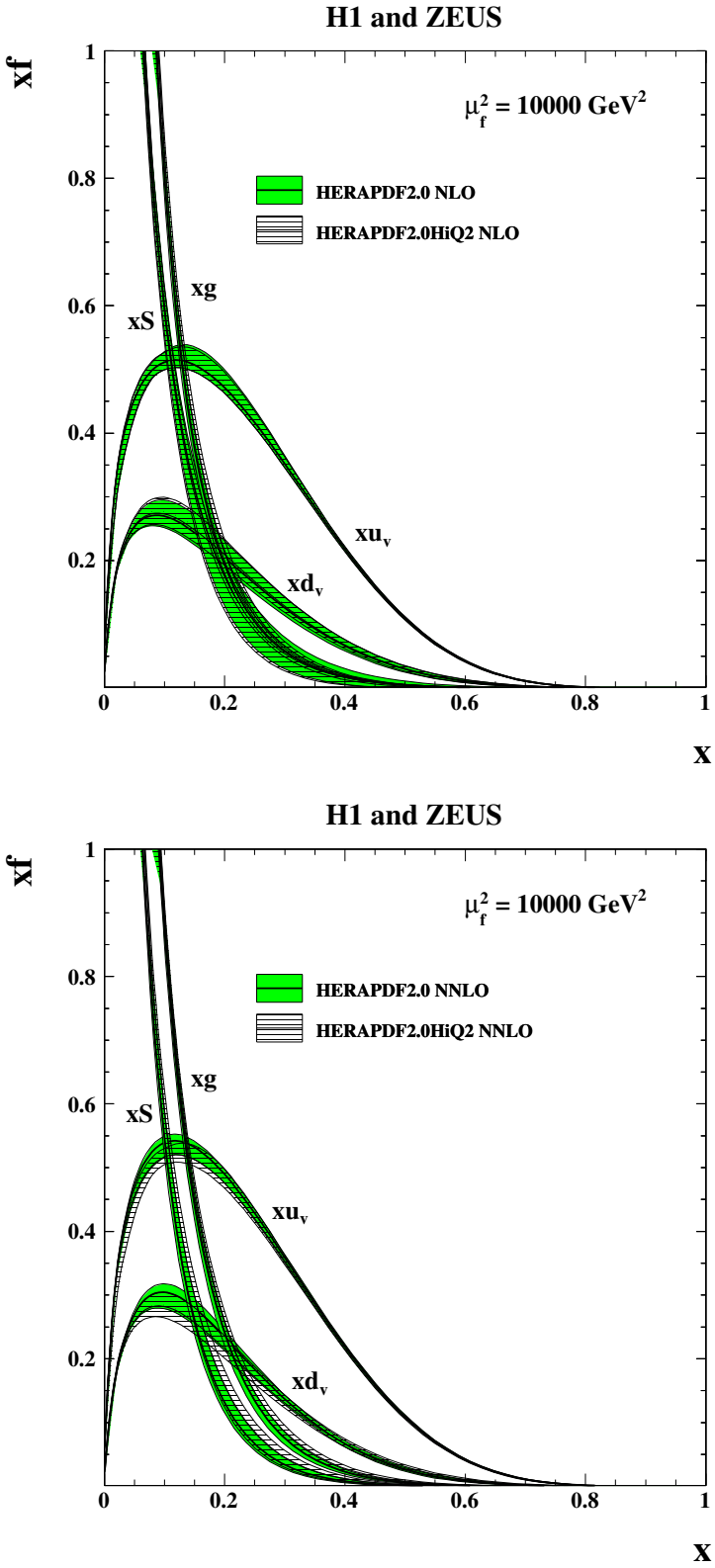

Figure 6: The parton distribution functions of HERAPDF2.0, xu_v, xd_v, $xS = 2x(\bar{U}+\bar{D})$, xg, at $\mu_f^2 = 10000\,\mathrm{GeV}^2$ with $Q^2_{\mathrm{min}} = 3.5\,\mathrm{GeV}^2$ compared to the PDFs of HERAPDFHiQ2 with $Q^2_{\mathrm{min}} = 10\,\mathrm{GeV}^2$. Top for the NLO fits; bottom for the NNLO fits

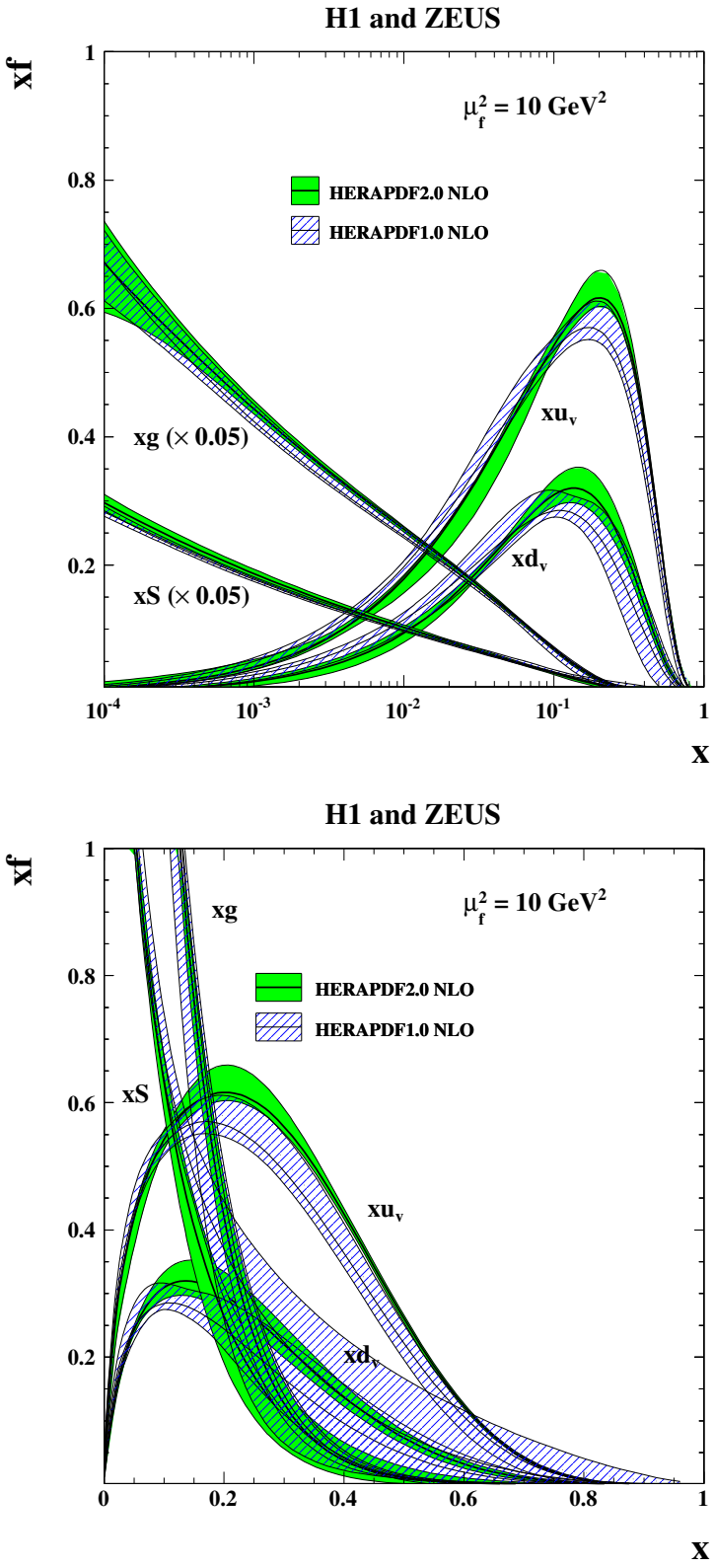

Figure 7: The parton distribution functions of HERAPDF2.0 NLO, xu_v, xd_v, $xS = 2x(\bar{U}+\bar{D})$, xg, at $\mu_f^2 = 10\,\mathrm{GeV}^2$ compared to HERAPDF1.0NLO on log (top) and linear (bottom) scales.

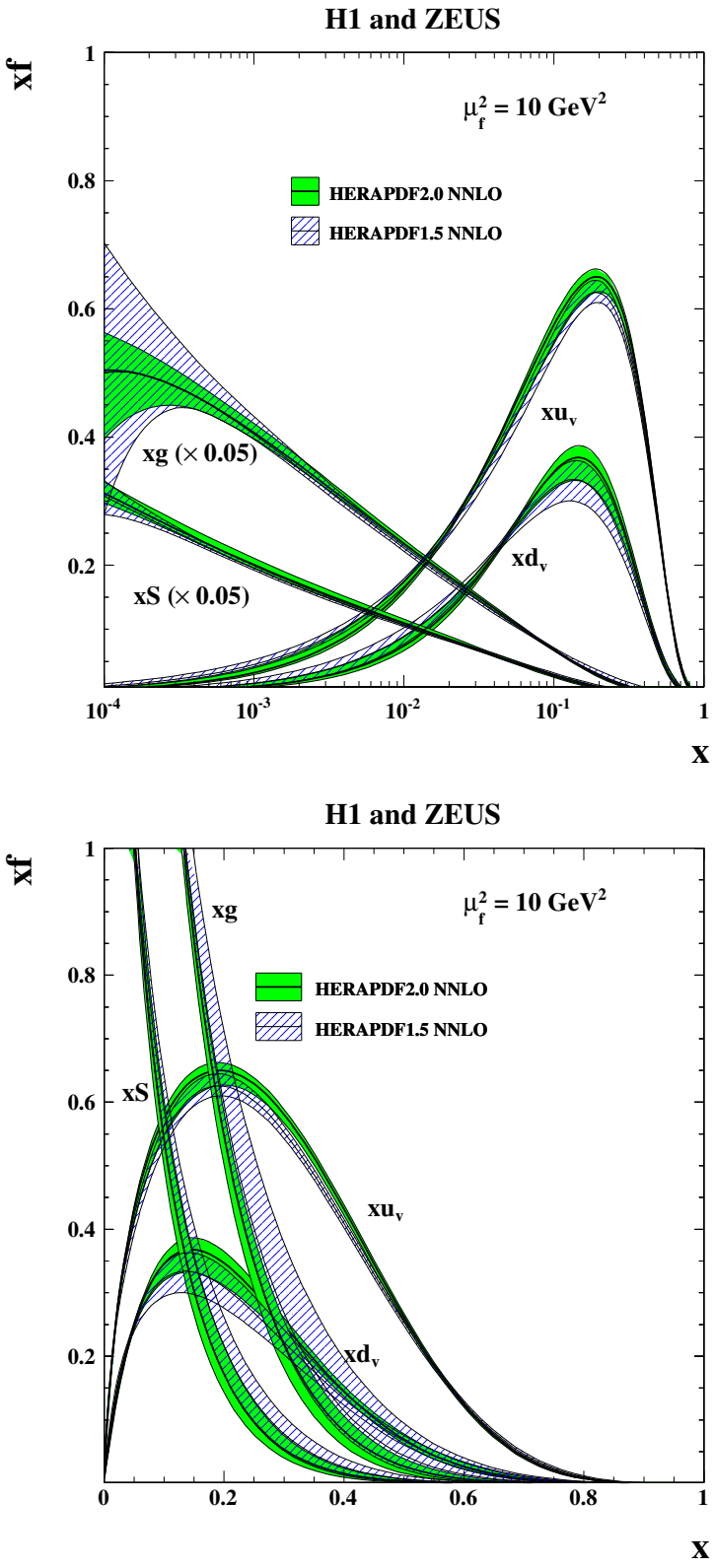

Figure 8: The parton distribution functions of HERAPDF2.0 NNLO, xu_v, xd_v, $xS = 2x(\bar{U}+\bar{D})$, xg, at $\mu_f^2 = 10\,\mathrm{GeV}^2$ compared to HERAPDF1.5 NNLO on log (top) and linear (bottom) scales.

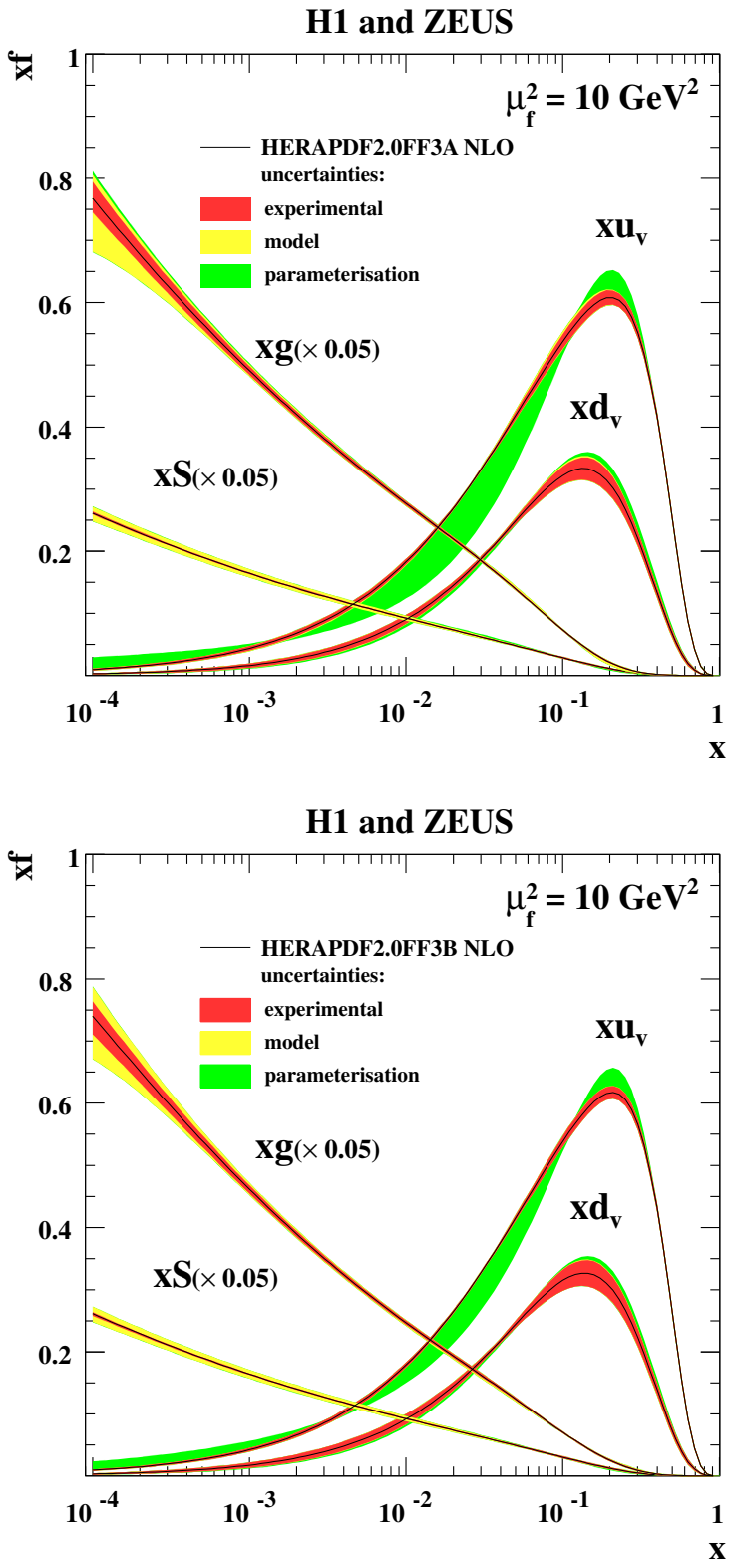

Figure 9: The parton distribution functions of HERAPDF2.0FF3A NLO and HERAPDF2.0FF3B NLO, xu_v,xd_v,xS=$2x(\bar{U}+\bar{D})$,xg, at $\mu_f^2 = 10\,\mathrm{GeV}^2$. The experimental, model and parameterisation uncertainties are shown separately.

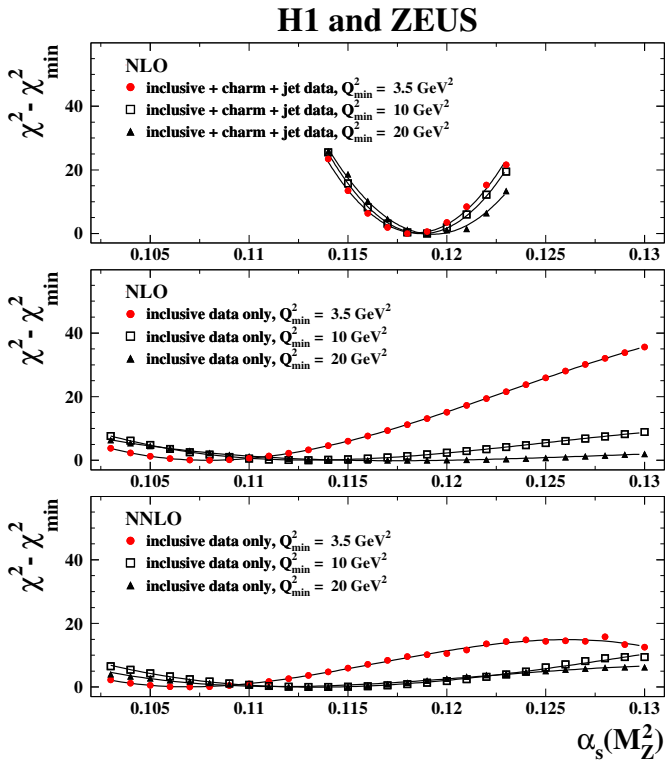

Figure 10: $\Delta\chi^2$ vs. $\alpha_s(M_Z^2)$ for pQCD fits with different $Q^2_{\rm min}$ using data on (a) inclusive, charm and jet production at NLO, (b) inclusive ep scattering only at NLO, and (c) inclusive ep scattering only at NNLO.

and the PDFs are available on https://www.desy.de/h1zeus/herapdf20.

References

[1] URL https://wiki-zeuthen.desy.de/HERAverager

[2] A. Glazov *et al*, [arXiv:1410:4412] URL https://www.herafitter.org

[3] H1 and ZEUS Collaboration, H. Abramowicz *et al*, [arXiv:1506.06042]

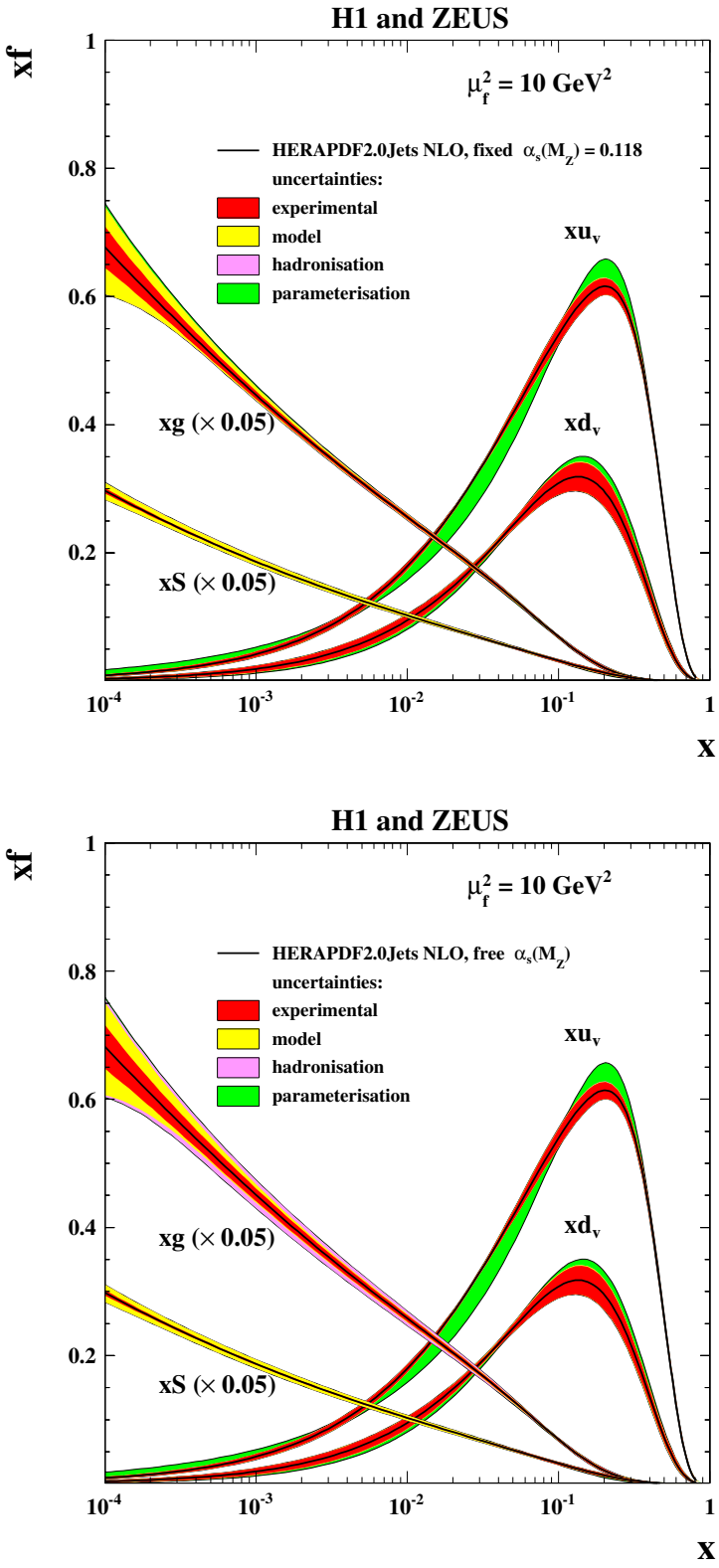

Figure 11: The parton distribution functions of HERAPDF2.0Jets NLO, xu_v, xd_v, $xS = 2x(\bar{U}+\bar{D})$, xg, at $\mu_f^2 = 10\,\mathrm{GeV}^2$ with fixed $\alpha_s(M_Z^2) = 0.118$ (top) and free $\alpha_s(M_Z^2)$ (bottom). The experimental, model and parameterisation uncertainties are shown separately. The hadronisation uncertainty is also included, but it is only visible for the fit with free $\alpha_s(M_Z^2)$.